Role of Silane Crosslinking on the Properties of Melt Blended Metallocene Polyethylene-*g*-Silane/Clay Nanocomposites at Various Clay Contents

W.-C. Chen,[1] S.-M. Lai,[2] Rong Yu Qiu,[3] Shi-Xian Tang[3]

[1]*Department of Chemical Engineering, Chinese Culture University, Taipei 111, Taiwan, Republic of China*
[2]*Department of Chemical and Materials Engineering, National I-Lan University, I-Lan 260, Taiwan, Republic of China*
[3]*Institute of Materials Science and Nanotechnology, Chinese Culture University, Taipei 111, Taiwan, Republic of China*

Received 25 October 2009; accepted 11 June 2011
DOI 10.1002/app.35261
Published online 2 November 2011 in Wiley Online Library (wileyonlinelibrary.com).

ABSTRACT: A study to investigate matrix properties and their interaction with loaded nanoclay was designed under controlled clay dispersion. Metallocene polyethylene grafted vinyltriethoxy silane (mPE-*g*-silane) was served as the matrix, with or without silane crosslinking (grafting and post crosslinking with catalyst versus only grafting without catalyst), to assess the strength of commercial organoclay (20A)-filled nanocomposites prepared via a melt mixing. According to X-ray diffraction and transmission electron microscopy analyses, all nanocomposites achieved similar dispersion degrees at specific clay contents mainly due to the silane interaction with the dispersed clay via hydrogen bonding and/or chemical bonding. Chemical bonding of grafted silane with clay was inferred based on the slightly higher crosslinking degree with increasing clay content for crosslinked cases. For uncrosslinked cases, the crosslinking degree was virtually zero regardless of clay content. The dynamic mechanical properties revealed enhanced interaction between mPE-*g*-silane and clay with increasing clay content based on the increased glass transition temperatures. Young's modulus of nanocomposites with crosslinked cases showed higher values in comparison with uncrosslinked cases at a specific clay content, indicating the significance of matrix crosslinking effect and the effective interfacial interaction between silane and clay especially at higher clay content. To the authors' best knowledge, this is the first study which generally maintains similar clay dispersions through the effect of uncrosslinking (only grafting) and crosslinking (grafting and post crosslinking), and then probes the effect of matrix properties and interfacial interactions at the large deformation state (tensile test) and small deformation state (cutting test). © 2011 Wiley Periodicals, Inc. J Appl Polym Sci 124: 2669–2681, 2012

Key words: metallocene polyethylene; clay; nanocomposite; moisture crosslinking

INTRODUCTION

Nanocomposites developed through a hybrid of organic and inorganic materials and dispersed at the nanoscale may expand into new science and new applications.[1] Among these newly developed nanocomposites, polymer/clay systems have industrial applications due to their ability to endow synergistically advanced properties with relatively small amounts of clay loads. Pioneering work on these nanocomposites involving the nylon 6/montmorillonite (MMT) clay system was conducted by Toyota.[1–3] Since then, extensive research on numerous polymer/clay nanocomposite systems have been conducted. In general, to gain optimum nanocomposite performance, the interfacial interactions between the polymer matrix and dispersed clay moiety have been considered to be relatively significant.[4] However, it is not easy to attain high dispersion of organic modified clay within the nonpolar polymer matrix without the addition of compatibilizer. Thus, a compatibilizer is often employed to alleviate this problem.[5–8]

Metallocene polyethylene elastomer (mPE) is considered as a thermoplastic elastomer for its processing convenience. It can be also used as a conventional elastomer via a crosslinking process to meet the requirement of a low compression set (low permanent set) for crosslinked elastomers. For nanoclay filled nanocomposites, Kuo et al.[9] found that the crystallization rate increased with the incorporated nanoclay into the mPE matrix. However, Lew et al.[10] indicated that the incorporated clay tended to impede the lamellar crystallization for metallocene-based linear low density polyethylene (mLLDPE). For tensile properties, it has been reported that clay increased tensile strength by up to 40% for their

Correspondence to: S.-M. Lai (smlai@niu.edu.tw).
Contract grant sponsor: R.O.C. Government; contract grant number: NSC 96-2221-E-197-009.

© 2011 Wiley Periodicals, Inc.

mPE/clay system.[11] To obtain highly filled PE/clay nanocomposites, an *in situ* polymerization method including the methylaluminoxane-treated commercial Cloisite 15A was performed.[12] To enhance the clay dispersion, Lu et al.[13] and Wang et al.[14] prepared linear low density PE grafted silane/clay and high density PE nanocomposites to assist nanoclay dispersion, respectively, but there were no reports on the mechanical properties. Qian et al.[15] employed dodecyl-trimethoxylane modified clay to improve the miscibility of clay with low density PE matrix, involving the grafting reaction between the silane and silanol groups on the edge of clay. Our recent work on the mPE/clay via peroxide crosslinking with the help of maleated compatibilizer indicated that the maleated compatibilized nanocomposites conferred higher Young's Modulus, tensile strength, and tear strength than their counterparts without a compatibilizer, reflecting the increased interfacial interaction with the exploit of the compatibilizer.[16]

There have been numerous studies conducting on the applications of maleated compatibilizers in other polymer–clay nanocomposites to assist clay dispersion. For example, as evidenced by their PP/clay nanocomposites, Szazdi et al.[17] pointed out that high exfoliation may not guarantee high strength of layered silicate nanocomposites if PP-*g*-MA (polypropylene-*g*-maleic anhydride) with low molecular weight was used as a compatibilizer. Our recent work on styrene-ethylene-butylene-styrene block copolymer (SEBS)/clay nanocomposites, using styrene-ethylene-butylene-styrene block copolymer grafted maleic anhydride (SEBS-*g*-MA) and polypropylene grafted maleic anhydride (PP-*g*-MA) to assist clay dispersion, also supported this important finding.[18] It was suggested that matrix properties variation from the compatibilizer properties attributed to this unexpected decrement in mechanical properties even for the attained high exfoliation of clay within the matrix through the help of compatibilizer. To assess this phenomenon further, the compatibilizer could be directly used as the matrix for a control system containing only the compatibilizer and clay, in which the contributions to the mechanical properties from the compatibilizer properties or clay dispersion could be possibility justified. Our designed system of mPE-*g*-silane/clay system could be helpful for the in-depth understanding to the final performance when mPE-*g*-silane was used as a compatibilizer in other systems.

This work mainly attempts to further signify the importance of matrix properties and/or interfacial interaction under a similar clay dispersion degree by using functionalized polyolefin elastomer (mPE-*g*-silane), treated with or without the silane crosslinking effect (i.e., crosslinked versus uncrosslinked cases). This crosslinked system containing catalyst to effectively induce crosslinking was activated within a hot water bath. For comparison, mPE-*g*-silane mixed with clay without adding a catalyst, an uncrosslinked system, was also subjected to the hot water bath in a similar condition to give the same thermal process history as the crosslinked system. Without this designed treatment, the thermal history of uncrosslinked cases and crosslinked cases will have different thermal histories, which was then hard to compare. Thus, this work was carefully designed to consider this thermal effect often neglected in the literature. Through simple mixing to essentially achieve the same clay dispersion degree and with the help of silane interaction with clay, further silane crosslinking would not alter the clay dispersion, allowing us to signify the importance of matrix properties and/or interfacial interaction under a similar clay dispersion degree. To the authors' best knowledge, there is no available literature that discusses the contribution directly from the matrix properties variation from crosslinking effect, and/or its interfacial interaction with nanoclay at a similar clay dispersion degree designed at the same thermal history for mPE-*g*-silane/clay nanocomposites.

EXPERIMENTAL

Materials

The materials used in this study were mPE and commercial clay. At this stage, mPEs with a melt index of 1.0 g min^{-1} and molecular weight of 105,800 g mol^{-1} were procured from Du Pont Corp., under the trade name Engage 8003, corresponding to an octene comonomer content (%) of 30. The commercial organic modified montmorillonite (O-MMT) (Cloisite 20A, denoted as 20A in the following), obtained from Southern Clay Products, was used as received. The organic modifier agent was 2M2HT (dimethyl, dihydrogenated tallow, quaternary ammonium) as shown below:

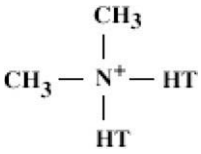

In the above, HT is hydrogenated tallow (~ 65 wt % C18; ~ 30 wt % C16; ~ 5 wt % C14). Initiator, dicumyl peroxide (DCP, 99% purity, First Chemical), vinyl triethoxy silane (VTEOS, Acros), and dibutyltin dilaurate (DBTL, TCI) were the reagent grades used to impart silane grafting of mPE, followed by a subsequent crosslinking.

Sample preparations

The grafting reaction of mPE with 3.5 phr (parts per hundred mPE resins) of silane containing 0.1 phr of

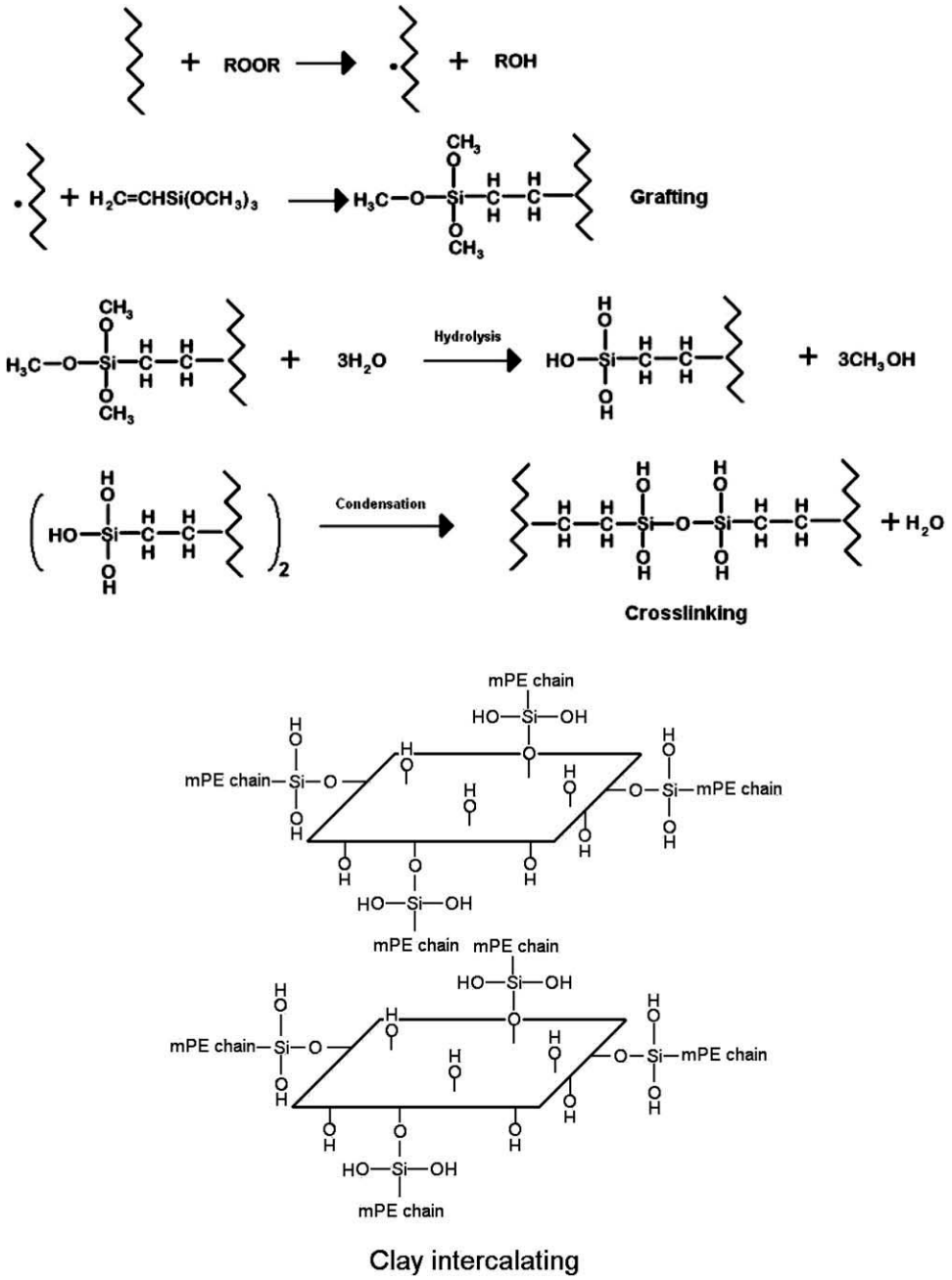

Figure 1 The moisture crosslinking and clay intercalating reaction scheme.

peroxide and 0.05 phr of DBTL catalyst was carried out using an internal mixer (P and L Industries), under 50 rpm for 10 min at 165°C. Noted that peroxide does not serve as a crosslinking agent here. For this silane grafting system, peroxide only served as an initiator especially for a small content of 0.1 phr. Further crosslinking is subjected to the condensation of the silanol group (Si—OH) to form siloxane crosslinks. The moisture assisted silane crosslinking reaction scheme[19] is shown in Figure 1. The catalyst employed here was used to speed up the silane condensation in the moisture crosslinking process. Without a catalyst, the gel content was virtually zero in our system. Sirisinha and Meksawat[20] studied the effects of various moisture crosslinking times that reached up to 300 h for mPE-*g*-silane without a catalyst at 70°C, indicating that roughly only 10% gel content was attained for 15 h of moisture crosslinking. Certainly, higher DCP content (say, 1 phr) would cause another side effect of C—C crosslinks, which is normally seen in a simple peroxide crosslinking system without silane and catalyst.

The mixing of mPE-*g*-silane with clay was performed with additional 5 more minutes following the addition of silane, peroxide, and catalyst for the preparation of mPE-*g*-silane. The mixed batch was

then transferred to a compression molding machine for a hot press at 165°C. About 1-mm thin sheet was obtained afterward. The prepared thin sheet was then subjected to be crosslinked in a water bath for 4 h at 70°C. This system containing catalyst was denoted as the crosslinked system. For comparison, mPE-*g*-silane prepared without adding a catalyst was mixed with clay, after which the compression molded sheet was subjected to a water bath in a similar condition to give the same thermal process history as the crosslinked system. This system without catalyst was denoted as the uncrosslinked system (without crosslinking) for a parallel comparison. After their preparation, the samples were left for at least 1 day in a vacuum drier before any measurements were done. Tensile test specimens complying with ISO-37 Type (III) standard were then prepared through a die cut. Cutting test specimens with a thickness of 1 mm were also prepared, with backing cloth at one side, to prevent an extension of sample legs under load.

Measurements

Using the Soxhlet extraction method, continuous extraction of crosslinked samples in boiling *p*-xylene (140°C) was carried out, corresponding to ASTM D 2765-90 method A. Molecular weight between crosslinks (M_c) were determined according to the literature[21]

$$M_c = -V\rho_p\{[(\varphi_p)^{1/3} - (0.5\varphi_p)]/[\ln(1-\varphi_p) + \varphi_p + x\varphi_p^2]\} \quad (1)$$

where V is the molar volume of xylene solvent molecule (122 $cm^3\ mol^{-1}$), φ_p is the volume fraction of polymer in the swollen gel ($[1+(\rho_p M_s/\rho_s M_d)]^{-1}$) with ρ_p as the polymer density (0.885 g cm^{-3}), ρ_s as the solvent density (0.866 g cm^{-3}), M_s and M_d as the weight of the polymer swollen with solvent and the dried polymer composite. In addition, Flory–Huggins interaction parameter, x, is represented as $V(\delta_s - \delta_p)^2/(RT)$, where, δ_s is the cohesive energy density of solvent (18.3 $MPa^{1/2}$), δ_p is the cohesive energy density of polymer (15.2 $MPa^{1/2}$), R is the universal gas constant (8.31447 J $k^{-1}\ mol^{-1}$), and T is the absolute temperature (298 K).

Structure and morphological characterizations

To evaluate the dispersion of O-MMT in the composites, X-ray diffraction (XRD), and transmission electron microscopy (TEM) were employed. A Siemens D5005 (Karlsruhe, Germany) X-ray unit, operating at 40 kV and 40 mA, was used to carry out the experiments. The X-ray source was Cu K_α radiation with a wavelength of 0.154 nm. The diffractograms were scanned in the 2θ range 2–26°, at a rate of 1° min^{-1}. Using a JEOL JEM-1230, TEM analysis was performed on ultrathin sections of cryo-microtomed thin films at an acceleration voltage of 100 kV.

Thermal characterization

The sample was first heated to 150°C at 20°C min^{-1}, using a DSC (Perkin–Elmer DSC 7) to eliminate the sample thermal history. Afterward, the sample was cooled to 0°C with a cooling condition of 10°C min^{-1} for crystallization. The melting temperature (T_m) was measured at a heating rate of 20°C min^{-1} from 0 to 150°C. The glass transition temperature (T_g), was determined via a dynamic mechanical analyzer DMA (Perkin–Elmer, DMA Diamond), under a tensile mode at a frequency of 1 Hz and a heating rate of 5°C min^{-1} from −80 to 30°C. Thermogravimetric analysis (TGA; Perkin–Elmer, TGA6) was used to evaluate the thermal stability of the composites. The heating rate of 20°C min^{-1} was used, from 30 to 750°C within a nitrogen environment.

Mechanical properties

Tensile measurements were conducted based on ASTM-D638, at a crosshead speed of 20 cm min^{-1}, using a Universal Tensile Testing Machine (QC-506A1). Tensile strength, elongation, and Young's modulus were all recorded. In addition, cutting test was also employed to measure the fracture energy (G_c) using a razor blade at a cutting speed of 10 mm min^{-1} around room temperature. The schematic sketch of the out-of-plane cutting test is shown in Figure 2. Pulling energy (P) and cutting energy (C) were calculated as follows[22,23]:

$$P = 2f_A(1-\cos\theta)/t \quad (2)$$

$$C = f/t \quad (3)$$

In the above, f_A is the suspended load on the two legs of test specimens, f is the cutting force required to cut through samples, and 2θ and t, represent the angles between two legs, and cut thickness, respectively.

By measuring the cutting force and angle, the fracture energy G_c was calculated from the sum of energies expended in both pulling and cutting as presented below[22,23]:

$$G_c = P + C \quad (4)$$

RESULTS AND DISCUSSION

Properties of the uncrosslinked or crosslinked system for mPE-*g*-silane/clay nanocomposites at

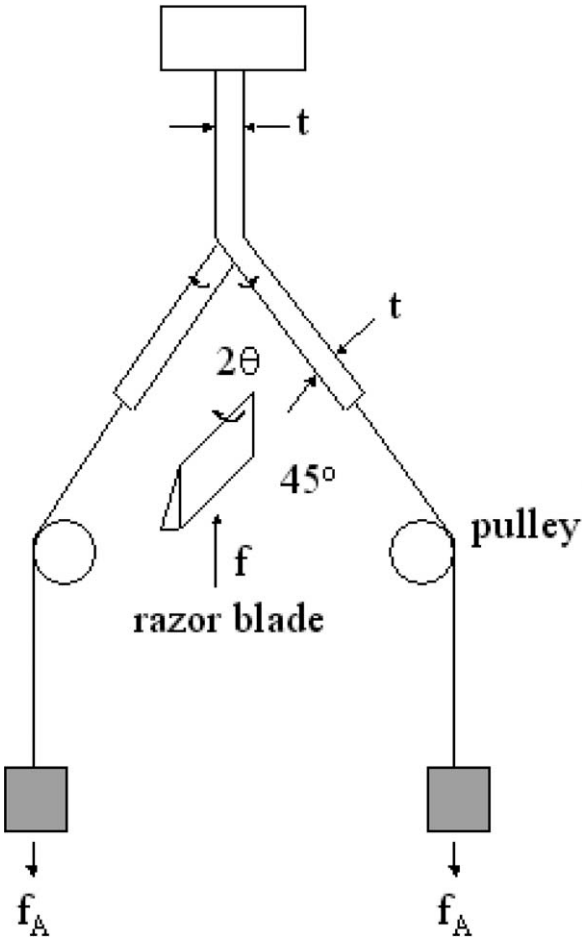

Figure 2 Schematic of cutting test.

various clay contents were investigated in the following sections. Moisture crosslinking was imparted to compare the interfacial effects between matrix and clay, as well as the matrix properties variation. Typical examples of mPE-*g*-silane/clay (crosslinked) nanocomposites are illustrated, because they showed the highest enhancement in Young's modulus, unless otherwise stated. Furthermore, the typical medium clay content at 5 phr is chosen for ease of comparison on the investigated system.

Structure characterization and dispersion assessment

Figure 3 shows XRD patterns of mPE-*g*-silane and its nanocomposites. A visible diffraction peak, corresponding to the interlayer spacing of 2.26 nm for 20A clay can be observed from Figure 3(a). When the mPE-*g*-silane/clay case (without crosslinking) was fabricated with a certain shear stress, generated from the rotors in the internal mixer, the peak intensity at 2 phr content was extremely weak, making it difficult to assess the clay dispersion. As stated in the literature,[24,25] the formation of exfoliated nanocomposites in a melt mixing technique is a combination of shear stress and molecular diffusion, through the peeling effect exerted on the stacked silicate platelets. However, the morphology subsequently determined via TEM suggested a good dispersion of clay (or swollen tactoids) at this low silicate content as well. Further, the position of the diffraction peak gave a slight shift of broad diffraction peak toward a smaller degree region at 5 and 9 phr clay. Additionally, upon examining the diffraction peak at a higher degree region, the crystalline structure of mPE-*g*-silane was not altered by the incorporated clay. To better reveal the crosslinking effect, the results are shown in Figure 3(b) for the mPE-*g*-silane/clay (crosslinked) case. Further moisture crosslinking yielded similar or slightly smaller diffraction angles in comparison with previous cases, indicating a good dispersion of clay or swollen tactoids with slightly similar degrees of interaction between clay and silane grafted matrix. Noted that, Lu et al.[13] prepared linear low density PE (LLDPE) grafted silane/clay nanocomposites via the reactive extrusion method by adding vinyl trimethoxy silane, dicumyl peroxide, 5 phr hexadecyl trimethyammonium bromide (C16) modified clay together with LLDPE and found that the *d*-spacing increased from 2.5 nm of O-MMT to 3.4 nm of the LLDPE-*g*-silane/clay system with higher thermal-oxidative stability. Wang et al.[14] prepared high density PE (HDPE) grafted silane/clay nanocomposites and found that the diffraction peak at $2\theta = 2.3^\circ$ ($d = 3.84$ nm) for 2 or 4 wt % modified clay dispersed in HDPE-*g*-silane matrix. Both papers led to a similar *d*-spacing in comparison with our systems, however there were no reports on the mechanical properties of their nanocomposites and the comparison of systems without crosslinking (only grafting) and crosslinking (grafting and post crosslinking) as we investigated in this work. Our previous work on the preparation of mPE/clay via a peroxide curing system indicated that the *d*-spacing of clay increased with the addition of mPE-*g*-MA compatibilizer. The comparison for the peroxide curing system was mainly on the effectiveness of compatibilizer, rather than the effect of crosslinking. Thus, the comparison here is only for the reference.

For the comparison between uncrosslinked (only grafting) and crosslinked cases (grafting and post crosslinking) in Figure 3, although the *d*-spacing listed for uncrosslinked cases can be found as being slightly smaller than those for crosslinked cases at 5 and 9 phr, in the previous cases, the peaks were somewhat broad, with a secondary tiny peak at smaller angles close to those for the later cases. Thus, the dispersion degrees for both cases didn't vary much, and the detail dispersion should be elucidated with the aid of TEM analyses discussed below. In general, this finding signified the importance of enhanced interfacial reaction through the clay and silane-grafted matrix.

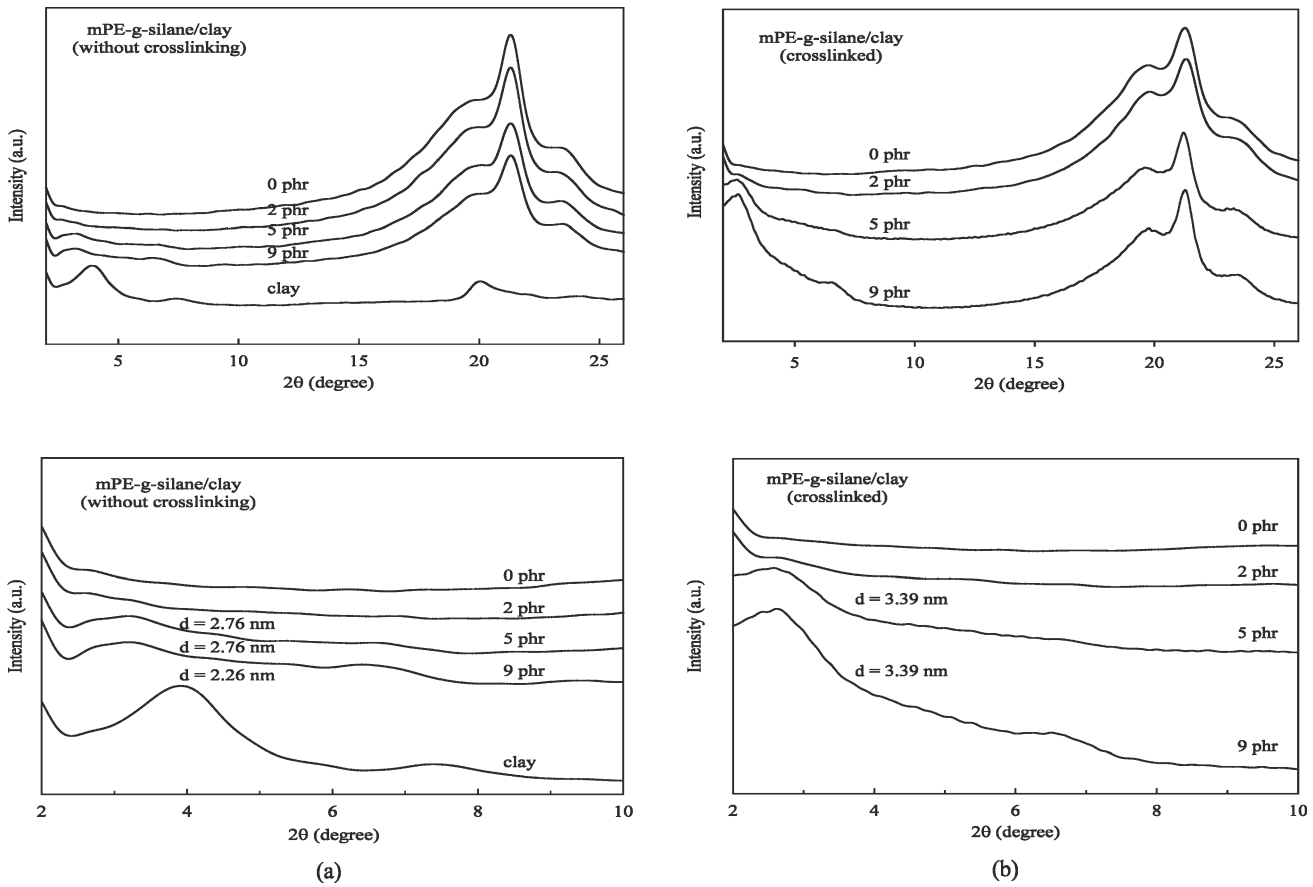

Figure 3 X-ray diffraction patterns of mPE-*g*-silane/clay (a) without crosslinking 2θ at 2°–26° and 10°, (b) crosslinked, 2θ at 2°–26° and 10°.

Figures 4 and 5 show TEM micrographs of mPE-*g*-silane nanocomposites including mPE-*g*-silane/clay (without crosslinking) and mPE-*g*-silane/clay (crosslinked) at various clay contents and magnifications. The dark lines (or stacked silicate platelets) represent clay tactoids, and the gray base represents the mPE-*g*-silane matrix. In Figure 4(a), a well-dispersed clay image can be found for mPE-*g*-silane/clay nanocomposites without crosslinking, except for some stacked silicate platelets portions. The original clay agglomerates are seen to be dispersed into a multi-layered structure, indicating that a uniform nanoscale has been attained. Figure 4(b) shows the clay dispersion status through the silane modification on mPE matrix with crosslinking. Basically, all images displayed fairly well-dispersed clay, with dark lines within the mPE-*g*-silane matrix. However, some stacked silicate platelets can also be found in the previous uncrosslinked cases. Figure 5 shows the higher magnification, thereby exhibiting similar findings. The uncrosslinked cases appeared to be in a similar degree with the crosslinked cases in assisting clay dispersion, which is in close agreement with our XRD analysis investigation. This suggests that the difference in clay dispersion between crosslinked and uncrosslinked cases is limited.

Thermal behaviors

As revealed from the XRD results, the crystal form of mPE-*g*-silane, with or without clay, was not greatly influenced. It is interesting to see how the crystallization and melting behaviors of the samples varied with the above effects. The crystallization peak temperature value (T_c, temperature at the exotherm minimum) of mPE-*g*-silane without crosslinking was about 62.6°C (Table I). Not much difference was found for the clay incorporated cases at various clay contents. Although clay normally acted as an effective nucleating agent to enhance crystallization, other factors such as shielding/miscibility could discount this positive effect.[26,27] Silane-modified mPE appeared to have a slightly higher crystallization temperature than mPE due to nucleation through added ingredients or grafted silane.[28] To show a brief comparison here, pure mPE was tested and a measurable difference of up to 5.0°C was found for both mPE (57.6°C) and mPE-*g*-silane (62.6°C; Table I). This indicates that the promotion of crystallization kinetics through the addition of clay moiety is limited due to increased compatibility between mPE-*g*-silane and clay in comparison with their pristine mPE and clay system. As for the mPE-*g*-silane/

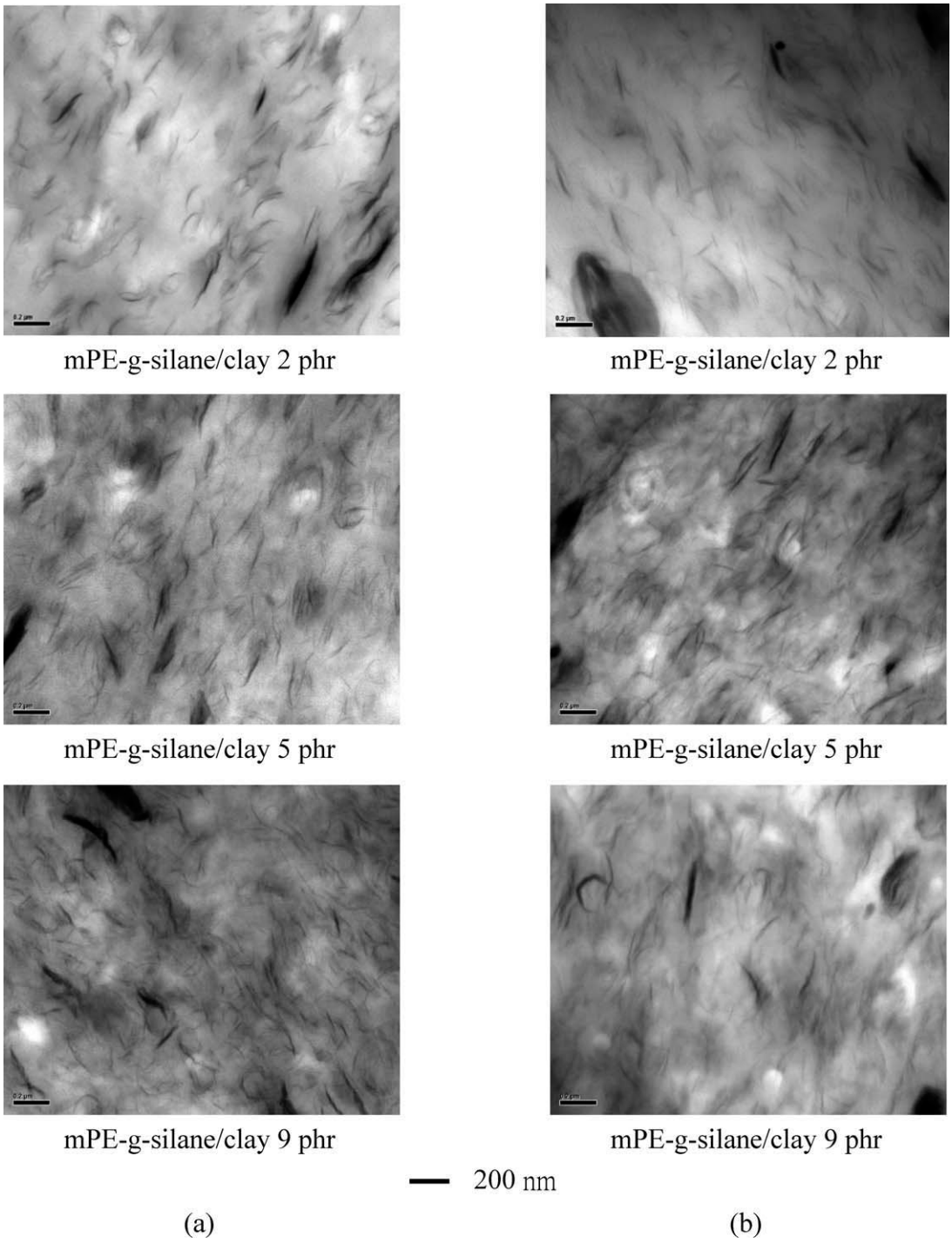

Figure 4 TEM micrographs of mPE-*g*-silane/clay at 50 K magnification (a) without crosslinking (2, 5, 9 phr), (b) crosslinked (2, 5, 9 phr), (scale bar: 200 nm).

clay system, a similar observation was found in that the effect of crosslinking on the crystallization temperature was rather limited. A comparison of the crystallization behaviors at a typical clay content of 5 phr showed no much difference as well (not shown here for brevity). Table I shows the comparison of T_c for all investigated cases. Noting that the moisture crosslinking process was performed at a temperature lower than the melting temperature (a solid state crosslinking, not crosslinking in the melt state), it was suggested that this type of crosslinking preferentially took place on the amorphous regions of the materials,[29] rendering limited difference in the thermal behaviors. As the thermal scan curves were broad, a small variation in the selection of integration baseline may show some difference in the

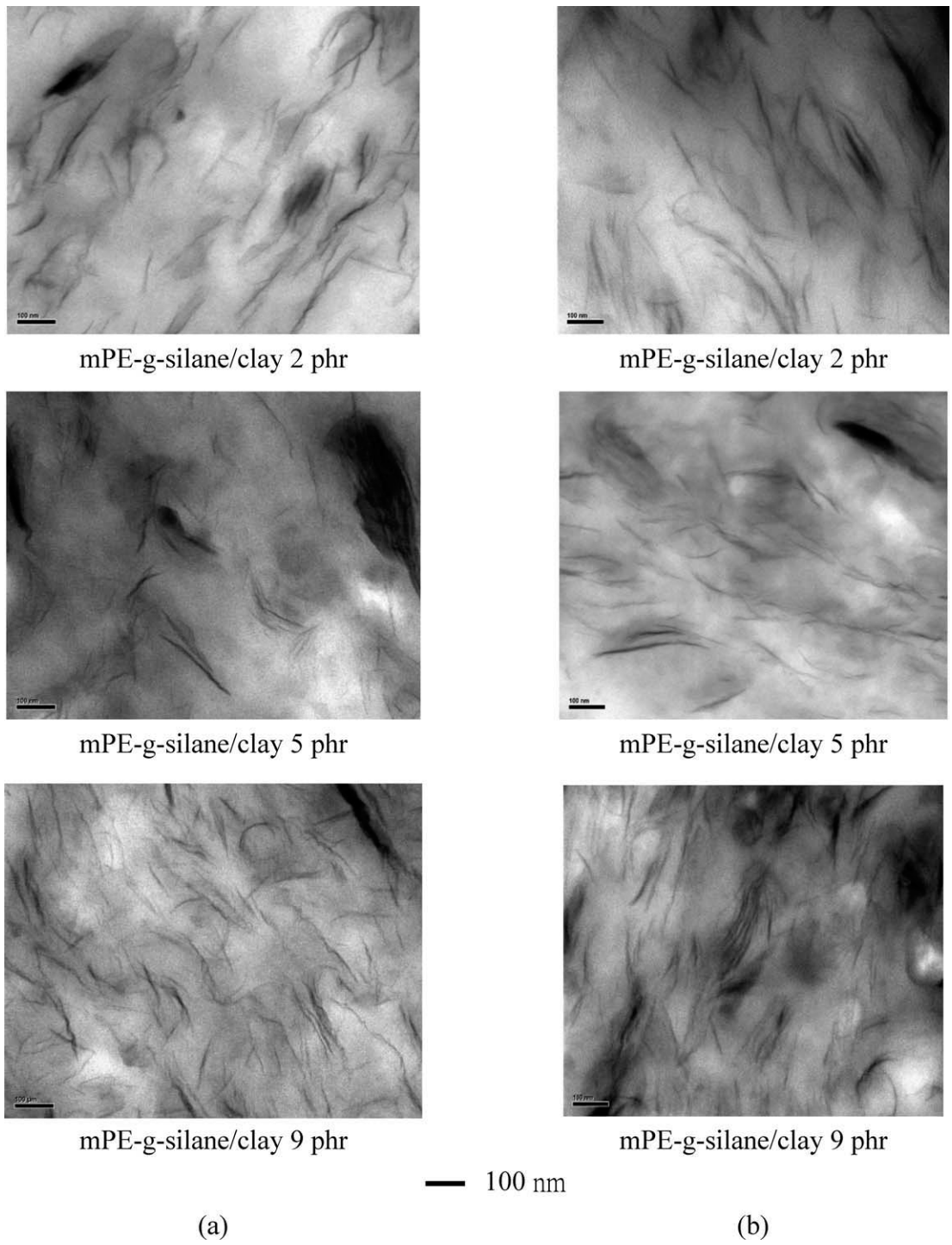

Figure 5 TEM micrographs of mPE-*g*-silane/clay at 100 K magnification (a) without crosslinking (2, 5, 9 phr), (b) crosslinked (2, 5, 9 phr), (scale bar: 100 nm).

crystallinity values. In considering this experimental difficulty, the observed differences in the crystallinity were not taken into account.

Results of melting points are shown in Table I for all investigated cases. For mPE-*g*-silane without crosslinking at 5 phr clay, the melting point is seen to be about 76.7°C, which is about the same as that of mPE-*g*-silane resin with crosslinking at the same clay content at about 76.1°C. Measurements were carried out for the other formulation including the silane-modified system. In Table I, no distinct effects from both the crosslinking effect and clay content can be seen. This suggests that the structure and crystal formation of mPE-*g*-silane were not affected (with or without clay), as seen in the XRD patterns.

TABLE I
Thermal Analysis of mPE-*g*-Silane/Clay Nanocomposites

Sample code	Clay (phr)	T_c (°C)	T_m (°C)	T_g (°C)
mPE-*g*-silane/clay (without crosslinking)	0	62.6	77.1	−30.3
	2	61.8	76.7	−27.1
	5	61.4	76.7	−26.6
	9	61.0	77.7	−22.0
mPE-*g*-silane/clay (crosslinked)	0	59.1	76.1	−30.3
	2	59.0	76.1	−27.1
	5	60.3	76.1	−27.8
	9	60.1	77.8	−25.5

T_m: The melting temperature at a heating rate of 20°C min^{-1}. T_c: The crystallization temperature at a cooling rate of 10°C min^{-1}. T_g: The glass transition temperature at a heating rate of 5°C min^{-1}.

Viscoelastic behaviors for the uncrosslinked or crosslinked system for mPE-*g*-silane/clay nanocomposites were assessed using a dynamic mechanical analyzer. The results for the crosslinked cases at various clay contents are shown in Figure 6. As can be seen, the glass transition temperatures of mPE-*g*-silane slightly increased, with the clay contents from 0 phr clay (−30.3°C) to 9 phr (crosslinked, −25.5°C). Furthermore, with increasing clay content, the tan δ values in the glass transition regions decreased slightly, indicating effective clay reinforcement and an increased mutual interaction for the nanocomposites.[30] Other investigated systems also displayed similar behaviors; the glass transition temperature result is listed in Table I for a quick comparison, which suggested a certain interaction between mPE-*g*-silane and clay-involved hydrogen bonding (evidently) and/or chemical bonding with supporting literature Ref. [13] as well. Basically, the silane crosslinking effect on the glass transition temperatures was marginal, indicating that the segmental motion of base resin was not significantly varied with crosslinking, but varied with the addition of clay. In particular, the uncrosslinked cases gave virtually zero gel content, but crosslinked cases conferred high gel content, as discussed earlier. To compare the gel content and DMA results, most likely, uncrosslinked cases involved only hydrogen bonding, but crosslinked cases involved hydrogen bonding and/or chemical bonding between clay and mPE-*g*-silane.

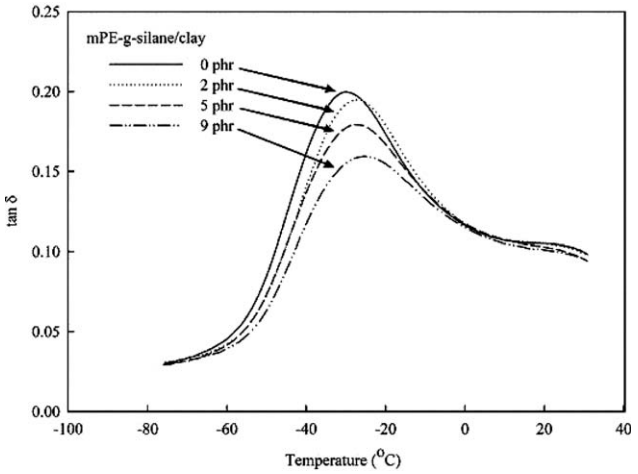

Figure 6 Tan δ of mPE-*g*-silane/clay (crosslinked) at various clay contents.

Thermal stability

To investigate the thermal stabilities of mPE-*g*-silane/clay nanocomposites, TGA was conducted and the results are shown in Table II. Two main features were observed here. First, not much crosslinking effect was found for the thermal properties of nanocomposites. The higher crosslinking degree did not always attain higher thermal stability. In their works, Marcilla et al. and Khonakdara et al. demonstrated slightly reduced trends at the onset of thermal decomposition, with increasing peroxide content in their peroxide crosslinked polyethylene systems; this can be attributed to the presence of higher concentrations of tertiary carbons that have been induced by crosslinking and are less stable thermally.[31,32] However, they also mentioned these

TABLE II
Thermal Degradation Temperatures of mPE-*g*-Silane/Clay Nanocomposites

		Weight loss temperature (°C) at the loss of		Degraded temperature	Ash content
Sample code	Clay (phr)	5 wt %	50 wt %	T_{max} (°C)	wt %
mPE-*g*-silane/clay (without crosslinking)	0	425.1	460.0	463.2	1.3
	2	426.0	469.9	472.3	2.2
	5	425.1	460.3	463.9	4.3
	9	424.5	460.7	461.9	6.7
mPE-*g*-silane/clay (crosslinked)	0	417.9	459.6	465.2	1.9
	2	430.8	473.1	477.2	2.4
	5	423.9	462.7	465.3	4.5
	9	427.2	464.0	465.6	6.9

differences were almost negligible, and all crosslinked and uncrosslinked polyethylene showed very close behaviors regardless of the amount of gel content. Table II shows the representative index of thermal stability, in which it appears that 2 phr clay loaded cases for the uncrosslinked or crosslinked system exhibited slightly higher thermal stability, perhaps due to a higher degree of dispersion for this lower clay content. However, the difference in other clay loaded cases was rather limited in terms of complex thermal degradation effect wherein clay content effect was considered to be marginal at high clay content, especially for higher content of intercalant with low thermal stability within clay gallery. Second, the residual ash content for nanocomposites fell in the range of 2.2–6.9 wt %, close to the amount of loaded clay. Two competing effects may account for this observation, as clay may serve as a heat barrier to induce higher ash content for the organic resin; however, the loss of intercalant within the clay gallery discounted the actual clay content. In general, no significant difference was found at the high weight loss ranges, indicating the limited influence of silane modification and loaded clay on the degradation behavior of the prepared nanocomposites. This can be mainly attributed to the lack of extensive exfoliation of clay.

Mechanical properties: Tensile properties and cutting strength

As discussed above, both crosslinked and uncrosslinked cases could achieve a similar dispersion degree of clay tactoids, as determined through XRD and TEM analysis. It is interesting to see how both crosslinking and clay effect influence the tensile properties of nanocomposites as illustrated in Figure 7. Figure 7(a) depicts Young's modulus of composites, wherein it can been that the Young's modulus of pristine mPE-g-silane without crosslinking is about 24.4 ± 1.6 MPa, and that the value for the nanocomposites increased up to the maximum value of 36.8 ± 0.5 MPa at 5 phr clay mainly due to the reinforcing effect of organic treated clay. Additionally, the Young's modulus of nanocomposites with crosslinked case, showed higher values in comparison with uncrosslinked cases investigated at specific clay contents, indicating the significance of the matrix crosslinking effect and effective interfacial interaction between silane and clay especially at higher clay content. Note that the relatively high degree of clay dispersion observed in PP-*g*-MA compatibilized PP/clay nanocomposites did not confer the highest measured tensile properties; to understand this mechanism, the matrix properties and types of compatibilizers employed between clay and matrix must be taken into account.[17,33] Our previous results suggested that the matrix properties and compatibilizer types are major factors in attaining the best nanocomposite performance in terms of tensile properties at a specific clay content.[18] As the dispersion degree did not vary using the current approach, the contribution in mechanical properties was mainly attributed to the interfacial interaction between the matrix and dispersed clay and/or matrix properties, especially at higher clay content.

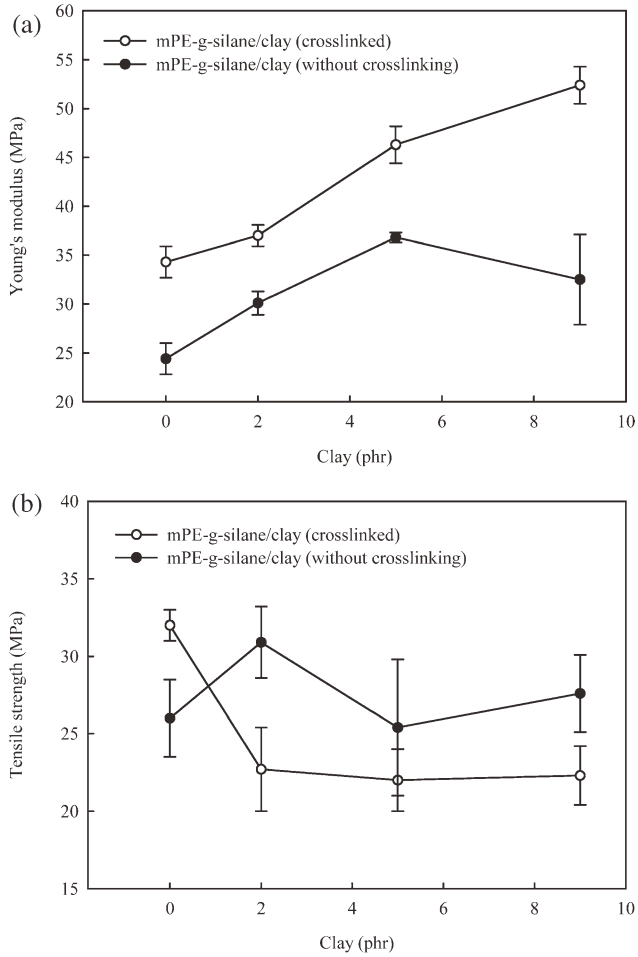

Figure 7 Tensile properties of mPE-*g*-silane/clay (a) Young's modulus, (b) tensile strength.

Further, Figure 7(b) shows the tensile strength for the uncrosslinked or crosslinked system. Here, tensile strength for mPE-*g*-silane with crosslinking was found to be higher than that without crosslinking, indicating a network formation to withstand the loading force at a large deformation. Our previous study[34] indicated a slight variation in tensile strength, depending on the crosslinking degree for the mPE-*g*-silane system. However, with the addition of clay, tensile strength did not increase further, which was not uncommon in some systems. In addition, different tensile strength levels for crosslinked cases were unexpectedly lower than those of uncrosslinked cases, which might be attributed to the

defects induced from microscale heterogeneity crosslinking or the higher crosslinking degree near the clay surface than the matrix as proposed by Mousa and Karger-Kocsis[35] in their styrene-butadiene rubber/clay system. In our work for the crosslinked system, the estimated molecular weight between crosslinks slightly decreased (i.e., increased gel content) from 17,057 ± 409 g mol^{-1} without clay corresponding to a gel content of 68.2% ± 8.4% to 14,983 ± 373 g mol^{-1} (70.8% ± 5.3%, 2 phr), 13,201 ± 343 g mol^{-1} (73.4% ± 7.0%, 5 phr), and 12,148 ± 343 g mol^{-1} (77.5% ± 8.1%, 9 phr), which reflected the slightly increased gel content for clay to serve as "apparent crosslink points" and could be attributed to mPE grafted silane to interact with clay.[13,14] Noted that the inevitable errors derived from the potential loss of clay, uncrosslinked chains trapped near clay during extraction, a possible profile of crosslinking degree in the thickness direction due to the clay interference with water diffusion, and the eq. (1) employed with some limitations, etc. would make this determination only a rough estimate. On the other hand, without a catalyst to induce crosslinking, the crosslinking degree was virtually zero in our system. Thus, the suggested uneven crosslinking would be the most probable factor to this observed decrement in tensile strength, especially with the addition of clay. As tensile strength is more sensitive to defects for a large deformation, in comparison with a small deformation in Young's modulus, this observed phenomenon could be considered peculiar, and the attained mechanical properties should be carefully evaluated to exploit the reinforcement of nanocomposites for certain applications.

Another way of understanding the fracture behaviors of mPE-*g*-silane nanocomposites is to confine their deformation in a nanoscale using a cutting test design. To further confine the crack tip diameters at a nanoscale using a sharp razor blade, cutting strength was evaluated. A slope of −1 was successfully draw, to obtain cutting strength of 580 ± 79 (J m^{-2}) for mPE-*g*-silane (without crosslinking; omitted here for brevity). More measurements toward the comparison of cutting strength are depicted in Figure 8. The cutting strength of crosslinked cases was only about 4% larger compared with uncrosslinked cases at various clay contents. The highest value attained was ∼ 675 ± 63 (J m^{-2}). Thus, cutting strength in both cases are in a similar order within experimental errors. Note that rigid clay gallery, with a dimension of nanometer, was considerably smaller than that of the blade tip diameter. Thus, the crack induced by the blade should propagate through mPE-*g*-silane matrix and the interphase region. Although crosslinking was mostly effected within the interphase and matrix, the increased interfacial interaction or matrix crosslinking, which

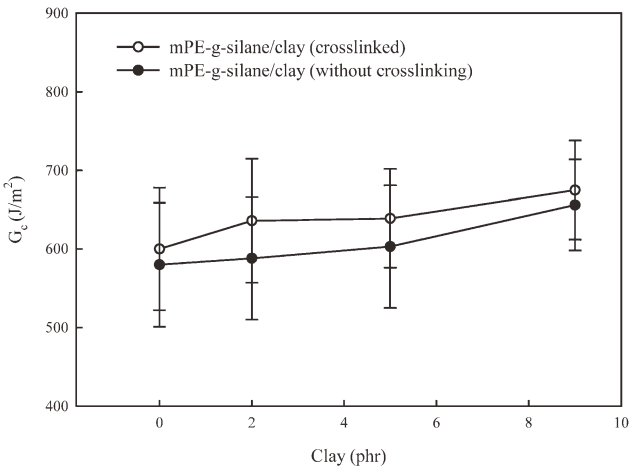

Figure 8 Cutting strength of mPE-*g*-silane/clay.

accounted for previous enhancements in tensile properties (Young's modulus), was limited by the control of blade tip. As a result, a relatively discernible crosslinking effect was observed. A similar observation was found for the effect of clay on cutting strength of nanocomposites. Cutting strength increased slightly with increasing clay content, with measurable experimental errors involving a maximum of 13% increment for mPE-*g*-silane/clay (9 phr), compared with mPE-*g*-silane in both crosslinked and uncrosslinked cases.

Although these values were not evaluated in the previous literature, they were comparable with other evaluations of cutting strength for different types of materials in the literature and our work such as high density polyethylene (HDPE),[36] SBR,[22] styrene-butadiene-styrene (SBS),[37] and polypropylene/ethylene–propylene–diene monomer thermoplastic vulcanizate (PP/EPDM TPV),[38] mPE.[34,39] For crystalline materials (LDPE and HDPE), higher values of cutting strength were obtained, suggesting that the crystalline yielding effect remained effective in dominating the cutting strength of material, even in a nanodeformation confined in a blade. On the contrary, for conventional amorphous elastomers without the crystalline effect (silicon rubber and SBR), lower values of cutting strength were normally found. Interestingly, thermoplastic elastomers (SBS, SEBS, and mPE) ranked in the intermediate order of cutting strength, in comparison with the above two types of materials. In particular, cutting strength seemed to increase slightly with increasing clay concentrations. Accordingly, induced micro-yielding and filler reinforcing effects from the blade were surmised to be possible. An attempt to suppress all the energy dissipations from micro-yielding of crystalline domains and filler reinforcement was not completely feasible in the current cutting design. However, it did reduce the zone of deformation to a certain degree, when compared

with tear measurements investigated, in our work on SEBS/clay nanocomposites.[40] Apparently, cutting strength was in a measure of the extent of dissipation around the tear tip. Interestingly, we further confirmed that nanoclay conventionally claimed for the enhancement of mechanical properties for general nanocomposites was found to be an insignificant role played in the confined deformation of materials on behalf of cutting design. Even though the clay dispersion state was similar through the current design, the strength of investigated nanocomposites was clearly dominated by those aforementioned dissipation processes; thus, these should be carefully defined in terms of large deformation, such as tensile test, or this nanofracture zone of small deformation in the cutting test.

CONCLUSIONS

This work mainly attempts to signify the importance of matrix properties and/or interfacial interaction under a similar clay dispersion degree by using functionalized polyolefin elastomer (mPE-*g*-silane), treated with or without the silane crosslinking effect serving as the matrix at various clay contents. This crosslinked system containing catalyst to effectively induced crosslinking was activated within a hot water bath. For comparison, mPE-*g*-silane mixing with clay prepared without adding a catalyst was also subjected to the hot water bath in a similar condition to give the same thermal process history as the crosslinked system. Thus, this study investigated the thermal and mechanical properties of nanocomposites for the dispersed commercial organoclay (20A) within the mPE-*g*-silane matrix at either uncrosslinked or crosslinked condition. According to the XRD and TEM results, the nanocomposites were achieved at a similar dispersion degree at specific clay contents. The glass transition temperatures of mPE-*g*-silane slightly increased with the clay contents, but the silane crosslinking effect on the glass transition temperatures was marginal. Chemical bonding of grafted silane with clay was inferred based on the slightly higher crosslinking degree with increasing clay content for crosslinked cases. For uncrosslinked cases, the gel content was virtually zero regardless of the clay content. To compare the gel content and DMA results, most likely, uncrosslinked cases involved only hydrogen bonding, but crosslinked cases involved hydrogen bonding and/or chemical bonding between clay and mPE-*g*-silane. Young's modulus of nanocomposites with crosslinked cases showed higher values in comparison with uncrosslinked cases investigated at specific clay contents. This indicates the significance of the variation of matrix properties, and the effective interfacial interaction between silane and clay especially at high clay content. In addition, tensile strength for crosslinked cases was unexpectedly lower than that of uncrosslinked cases, which might be attributed to the defects induced from the microscale heterogeneity crosslinking, a profile of crosslinking degree along thickness direction, or the higher crosslinking degree near the clay surface than the matrix. A relatively discernible crosslinking effect on the cutting strength was also observed. Cutting strength increased slightly with increasing clay content, with measurable experimental errors involved.

The tensile measurement, molecular weight between crosslinks, and reaction scheme from Jhong-Ren Chen and C.-H. Yang, respectively, are acknowledged.

References

1. Okada, A.; Usuki, A. Macromol Maters Eng 2006, 291, 1449.
2. Usuki, A.; Kojima, Y.; Kawasumi, M.; Okada, A.; Fukushima, Y.; Kurauchi, T.; Kamigaito, O. J Mater Res 1993, 8, 1179.
3. Kojima, Y.; Usuki, A.; Kawasumi, M.; Okada, A.; Kurauchi, T.; Kamigaito, O. J Polym Sci Polym Chem 1993, 31, 983.
4. Giannelis, E. P.; Krishnamoorti, R.; Manias, E. Adv Polym Sci 1999, 118, 108.
5. Osman, M. A.; Rupp, J. E. P.; Suter, U. W. Polymer 2005, 46, 1653.
6. Garcia, L. D.; Picazo, O.; Merino, J. C.; Pastor, J. M. Eur Polym Mater 2003, 39, 945.
7. Lopez-Quintanilla, M. L.; Sanchez-Valdes, S.; Ramos de Valle, L. F.; Medellin-Rodriguez, F. J. J Appl Polym Sci 2006, 100, 4748.
8. Dal Castel, C.; Pelegrini, T., Jr.; Barbosa, R. V.; Liberman, S. A.; Mauler, R. S. Compos A 2010, 41, 185.
9. Kuo, S.-W.; Huang, W.-J.; Huang, S.-B.; Kao, H.-C.; Chang, F.-C. Polymer 2003, 44, 7709.
10. Lew, C. Y.; Murphy, W. R.; McNally, G. M. Polym Eng Sci 2004, 44, 1027.
11. Maiti, M.; Sadhu, S.; Bhowmick, A. K. J Appl Polym Sci 2006, 101, 603.
12. Leone, G.; Bertini, F.; Canetti, M.; Boggioni, L.; Stagnaro, P.; Tritto, I. J Polym Sci Polym Chem 2008, 46, 5390.
13. Lu, H.; Hu, Y.; Li, M.; Chen, Z.; Fan, W. Compos Sci Tech 2006, 66, 3035.
14. Wang, H.; Fang, P.; Chen, Z.; Wang, S.; Xu, Y.; Fang, Z. Polym Int 2008, 57, 50.
15. Qian, Z.; Zhou, H.; Xu, X.; Ding, Y.; Zhang, S.; Yang, M. Polym Comp 2009, 30, 1234.
16. Lai, S.-M.; Chen, W.-C.; Wang, Z. W. J Polym Res 2011, 18, 1033.
17. Szazdi, L.; Pukanszky, B., Jr.; Vancso, G. J.; Pukanszky, B. Polymer 2006, 47, 4638.
18. Chen, W.-C.; Lai, S.-M.; Chen, C.–M. Polym Int 2008, 57, 515.
19. Sirisinha, K.; Meksawat, D. Polym Int 2005, 54, 1014.
20. Sirisinha, K.; Meksawat, D. J Appl Polym Sci 2004, 93, 901.
21. Adachi, K.; Hirano, T.; Kasai, P. H.; Nakamae, K.; Iwabukic, H.; Murakamic, K. Polym Int 2010, 59, 510.
22. Gent, A. N.; Lai, S.-M.; Nah, C.; Wang, C. Rubber Chem Technol 1994, 67, 610.
23. Lake, G. J.; Yeoh, O. H. J Polym Sci Polym Phys 1987, 25, 1157.
24. Fornes, D.; Yoon, P. J.; Keskkula, H.; Paul, D. R. Polymer 2001, 42, 9929.
25. Dennis, D.; Hunter, D. L.; Chang, D.; Kim, S.; White, J. L.; Paul, D. R. Polymer 2001, 42, 9513.

26. Lai, S.-M.; Chen, W.-C.; Zhu, X. S. Compos A 2009, 40, 754.
27. Nam, P. H.; Ninomiya, N.; Fujimori, A.; Masuko, T. Polym Eng Sci 2006, 46, 39.
28. Zhang, G.; Wang, G.; Zhang, J.; Wei, P.; Jiang, P. J Appl Polym Sci 2006, 102, 5057.
29. Sirisinha, K.; Meksawat, D. J Appl Polym Sci 2004, 93, 1179.
30. Nielsen, L. E.; Landel, R. F., Eds. Mechanical Properties of Polymers and Composites; Marcel Dekker: New York, 1994.
31. Marcilla, R.; Ruiz-Femenia, J.; Hernández, J. C.; Garcí-Quesada, J. Anal Appl Pyrolysis 2006, 76, 254.
32. Khonakdara, H. A.; Morshediana, J.; Wagenknechtb, U.; Jafari, S. H. Polymer 2003, 44, 4301.
33. Pukanszky, B. Eur Polym Mater 2005, 41, 645.
34. Lai, S. M.; Liu, J. L.; Chen, Y. C.; Chang, K. H. J Appl Polym Sci 2006, 101, 2472.
35. Mousa, A.; Karger-Kocsis, J. Macromol Mater Eng 2001, 286, 260.
36. Gent, A. N.; Wang, C. J Polym Sci Polym Phys 1996, 34, 2231.
37. Wang, C.; Chang, C. I. J Polym Sci Polym Phys 1997, 35, 2003.
38. Wang, C.; Chang, C. I. J Appl Polym Sci 2000, 75, 1033.
39. Lai, S. M.; Wu, T. H. J Polym Sci Polym Phys 2005, 43, 2207.
40. Lai, S.-M.; Chen, W.-C.; Chen, C.–M. Eur Polym Mater 2008, 44, 3535.